The current issue and full text archive of this journal is available on Emerald Insight at:
https://www.emerald.com/insight/0332-1649.htm

Model order reduction techniques applied to magnetodynamic T-Ω-formulation

Fabian Müller and Lucas Crampen
Institute of Electrical Machines, RWTH Aachen University, Aachen, Germany

Thomas Henneron
EEA, Université de Lille, Villeneuve-d'Ascq, France

Stephane Clénet
L2EP, Arts et Métiers ParisTech – Centre de Lille, Lille, France, and

Kay Hameyer
Institute of Electrical Machines, RWTH Aachen University, Aachen, Germany

Received 14 January 2020
Revised 11 April 2020
Accepted 13 April 2020

Abstract

Purpose – The purpose of this paper is to use different model order reduction techniques to cope with the computational effort of solving large systems of equations. By appropriate decomposition of the electromagnetic field problem, the number of degrees of freedom (DOF) can be efficiently reduced. In this contribution, the Proper Generalized Decomposition (PGD) and the Proper Orthogonal Decomposition (POD) are used in the frame of the T-Ω-formulation, and the feasibility is elaborated.

Design/methodology/approach – The POD and the PGD are two methods to reduce the model order. Particularly in the context of eddy current problems, conventional time-stepping algorithms can lead to many numerical simulations of the studied problem. To simulate the transient field, the T-Ω-formulation is used which couples the magnetic scalar potential and the electric vector potential. In this paper, both methods are studied on an academic example of an induction furnace in terms of accuracy and computational effort.

Findings – Using the proposed reduction techniques significantly reduces the DOF and subsequently the computational effort. Further, the feasibility of the combination of both methods with the T-Ω-formulation is given, and a fundamental step toward fast simulation of eddy current problems is shown.

Originality/value – In this paper, the PGD is combined for the first time with the T-Ω-formulation. The application of the PGD and POD and the following comparison illustrate the great potential of these techniques in combination with the T-Ω-formulation in context of eddy current problems.

Keywords Model order reduction, Proper generalized decomposition, Proper orthogonal decomposition, T-Ω-formulation, Finite element method

Paper type Research paper

1. Introduction

Because of its accurate representation of field quantities, the Finite Element Method (FEM) is commonly used to solve transient electromagnetic field phenomena by using the magnetic

This work was supported by the German Research Foundation (DFG) within the research project number 347941356 "Numerical Analysis of Electromagnetic Fields by Proper Generalized Decomposition in Electrical Machines."

COMPEL - The international journal for computation and mathematics in electrical and electronic engineering
© Emerald Publishing Limited
0332-1649
DOI 10.1108/COMPEL-01-2020-0025

vector potential formulation. However, another approach can be used by introducing the electric vector potential $\boldsymbol{T}$ and the magnetic scalar potential Ω, which lead to a smaller system while maintaining the accuracy. For eddy current problems, such as nondestructive testing, the $\boldsymbol{T}$-Ω-formulation is particularly suitable and superior to the magnetic vector potential formulation (Henneron *et al.*, 2007). To overcome the computational effort that arises owing to the solving of numerous linear equation systems, the model order reduction (MOR) is used. The Proper Orthogonal Decomposition (POD) is a widely used technique for MOR of large-scale systems and has been applied to electromagnetic field problems, among others, by Farzamfar *et al.* (2015), Henneron and Clenet (2013) and Henneron *et al.* (2015). A comparison between the commonly used magnetic vector potential formulation and the magnetic scalar potential formulation in combination with the POD can be found in Henneron *et al.* (2015). The Proper Generalized Decomposition (PGD) originates from the field of mechanical and fluid-dynamic problems (Nouy, 2010) (Chinesta *et al.*, 2011). It has shown its usefulness in facing numerous numerical challenges (Nouy, 2010), (Chinesta *et al.*, 2011), (Chinesta *et al.*, 2014), (Qin *et al.*, 2016a, 2016b) and has recently been applied to electromagnetic field computation in context with the magnetic vector potential formulation, inter alia, by Henneron and Clenet (2013), Qin *et al.* (2016a, 2016b) and Mueller *et al.* (2019a, 2019b). Owing to the advantages in terms of eddy current computation, using the PGD to the T-Ω method is yet to be done, and a first step toward fast simulation of eddy current problems such as nondestructive eddy current testing. To underline their importance and their processes, the PGD and the POD are declared in detail. Finally, the convergence and the computational effort of the two methods are exhibited.

2. Magnetodynamic finite element formulation

To apply the magnetic scalar potential formulation, the magnetic field strength needs to be defined by a combination of the magnetic scalar potential Ω and the electric vector potential $\boldsymbol{T}$ (1).

$$\boldsymbol{H} = \boldsymbol{T} - \nabla\Omega, \tag{1}$$

$\boldsymbol{T}$ is given by the sum of the exciting vector potential $\boldsymbol{T}_0$ and the eddy current constituent $\boldsymbol{T}_e$ (2).

$$\boldsymbol{T} = \boldsymbol{T}_0 + \boldsymbol{T}_e \tag{2}$$

By including Faraday's law, equations (1) and (2) result in equation (3) containing the unknown variables $\boldsymbol{T}_e$ and Ω.

$$\nabla \times \left(1/\sigma \nabla \times \boldsymbol{T}_e\right) + \partial \mu \boldsymbol{T}_e / \partial t - \partial \mu \nabla \Omega / \partial t = -\mu \partial \boldsymbol{T}_0 / \partial t \tag{3}$$

The second equation of interest, as stated in equation (4), originates from the junction of the magnetic flux density and the material equation for the magnetic field strength.

$$\nabla \cdot (\mu \boldsymbol{T}_e) - \nabla \cdot (\mu \nabla \Omega) = -\nabla \cdot \mu \boldsymbol{T}_0 \tag{4}$$

The exciting current vector potential is given by a spanning tree (Boehmer *et al.*, 2013). If a domain G contains a simply connected conductive region G_c, equations (3) and (4) can be

applied. The magnetic scalar potential is realized by nodal elements, whereas the electric vector potential is implemented in the edge element space. The Galerkin method is furthermore applied to obtain the weak formulation. A tree–cotree gauge is used in the conductive subdomain (Manges and Cendes, 1995).

3. Model order reduction

The methods of the POD and the PGD are based upon the theory that unknown potentials can be decomposed into products of functions, which depend on a spatial or temporal variable as shown in equation (5) (Henneron and Clenet, 2013), (Nouy, 2010), (Chinesta *et al.*, 2011), (Mueller *et al.*, 2019a, 2019b). In equation (5), $\boldsymbol{T}_e$, as well as $\boldsymbol{\Omega}$, are each represented by a vector U, and a finite amount m of terms, which are also frequently referred to as modes (Mueller *et al.*, 2019a, 2019b).

$$U \approx \sum_{i=1}^{m} \boldsymbol{R}_i(\boldsymbol{x}) S_i(t) \tag{5}$$

$\boldsymbol{R}$(x) is defined in the edge or nodal element space depending on the potential to be represented. S(t) is defined on the studied time interval.

3.1 Proper orthogonal decomposition

The *a-posteriori* reduction approach of the POD is based on taking necessary information from previous solutions in the reference system and the consecutive construction of a projection operator. This projection is applied onto the reference system to receive a reduced representation (Henneron and Clenet, 2013), (Henneron *et al.*, 2015), (Montier *et al.*, 2017).

3.1.1 Building the projection. To achieve a reduction in terms of degrees of freedom (DOF), the solution vector X, which contains $\boldsymbol{T}_e$ and $\boldsymbol{\Omega}$, is estimated with a new solution vector X_r of smaller size (Farzamfar *et al.*, 2015).

$$X \approx \boldsymbol{P} X_r, \tag{6}$$

where P denotes the projection operator which projects the system of size number of unknown n into a reduced system with the size m ($m \ll n$). The projection P is constructed by using the method of snapshots. The reference system is solved for k time steps, and the solutions are stored in the snapshot matrix $\mathbf{A}_S = [X_1, X_2, \ldots, X_k]$ of size $n \times k$, where k is equal to the number of snapshots (NoS). Furthermore, there are different strategies which m of those k calculated solutions should be taken to create the projection, shown in subsection 3.1.2. Consecutively, the resulting snapshot matrix $\mathbf{A}_S$ of size m has to be evaluated in terms of a singular value decomposition (SVD). For systems with many DOF, this leads to an ambitious computational effort. Using the relation between SVD of a given matrix $\mathbf{A}_S$ [equation (7)] and the eigenvalue decomposition of the correlated quadratic matrix C_S [equation (8)] (Henneron and Clenet, 2014), the computational effort is significantly reduced. Finally, the projection operator can be achieved by equation (9).

$$\mathbf{A}_S = \mathbf{V}\boldsymbol{\Sigma}\mathbf{W}^t \tag{7}$$

$$\mathbf{C}_S = \frac{1}{m}\mathbf{W}\Delta\mathbf{W}^t \tag{8}$$

$$\mathbf{P} = \mathbf{A}_S\mathbf{W} \tag{9}$$

Subsequently, to achieve the reduced system, the projection has to be applied to the reference equation:

$$\mathbf{P}^t\mathbf{M}\mathbf{P}\mathrm{X}_r = \mathbf{P}^t\mathbf{F}(t), \tag{10}$$

where $\mathbf{M}$ is the system matrix and F(t) is the right hand side, given by the weak forms of equations (3) and (4).

3.1.2 Snapshot method. A direct consequence of the projection creation [equation (9)] is the influence of the snapshots on the accuracy of the reduced system. By applying the SVD on the snapshot matrix, the solution space is explored. If the computed solutions, for example, contain the same vector twice or just a few very similar ones, the decomposition will not produce accurate results. The SVD extracts rotation and scaling given in the matrix $\mathbf{A}_S$, and for this reason mutually different snapshots are preferable. Two common routines for taking snapshots are illustrated in the following. The method with less computational effort is given by subsequently taking snapshots for a certain amount of time steps. As previously delineated, this method can lead to inaccuracies, if the snapshots are very similar.

The second method is the system-based approach. Owing to the transient behavior, the first m time steps will probably not sought all relevant information into the reduced model; therefore, taking evenly distributed snapshots will produce more accurate results. A trade-off between computational effort and accuracy is achieved by distributing the snapshots only in the first current period. For static problems, greedy algorithm-based snapshot methods can be used to further improve the decomposition but are unfeasible in terms of computational effort in context of eddy current problems (Mukherjee *et al.*, 2017). The two methods are exemplary depicted in Figure 1.

The snapshot method and the consecutive decomposition to achieve a projection operator do not depend on the formulation. In some cases, systems with multiple potentials such as the $\boldsymbol{T}$-Ω-formulation might suffer from bad representation by a single projection operator. To cope with this problem, one projection operator for each physical entity needs to be computed (Montier *et al.*, 2017). However, this issue did not occur in this research.

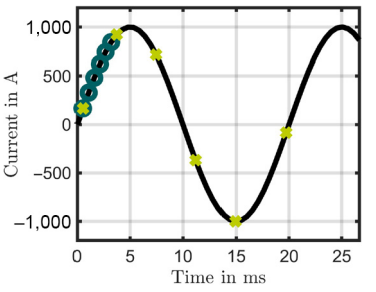

Figure 1.
Snapshots taken for the two presented methods: circle = sequential; cross = system-based

3.2 Proper generalized decomposition

The PGD is an *a priori* approach to achieve a separated form [equation (5)]. To use the general methodology developed in Nouy (2010), Chinesta *et al.* (2011) and Chinesta *et al.* (2014) to the $\boldsymbol{T}$-Ω-formulation, the two unknowns $\boldsymbol{T}_e$ and $\boldsymbol{\Omega}$ must be substituted by the approach outlined in equation (5) (Mueller *et al.*, 2019a, 2019b). In case of the weak formulation, the basic functions are substituted by equations (11) and (12). The nodal test function is indicated by α, whereas β typifies the edge element test functions.

$$\boldsymbol{\alpha}(\boldsymbol{x},\boldsymbol{t}) = \boldsymbol{R}_{\Omega}(\boldsymbol{x})'\mathrm{S}_{\Omega}(t) + \boldsymbol{R}_{\Omega}(\boldsymbol{x})S_{\Omega}(t)' \tag{11}$$

$$\boldsymbol{\beta}(\boldsymbol{x},\boldsymbol{t}) = \boldsymbol{R}_{\boldsymbol{T}}(\boldsymbol{x})'\mathrm{S}_{\boldsymbol{T}}(t) + \boldsymbol{R}_{\boldsymbol{T}}(\boldsymbol{x})S_{\boldsymbol{T}}(t)' \tag{12}$$

By presuming that the spatial or temporal function is known, the computation of the single modes is possible by applying an alternative direction scheme (Chinesta *et al.*, 2011). The test function, belonging to the known component vanishes in equations (11) and (12). As the modes up to $m-1$ are assumed to be known, the evaluation of the spatial function is done by using the FEM to solve the differential algebraic equations (13) and (14). $\boldsymbol{T}_{0,\mathrm{x}}/\mathbf{T}_{0,t}$ indicate the spatial and temporal part of the excitation as follows:

$$\begin{aligned}
&\sum_{\mathrm{i}=1}^{\mathrm{m}}\left(\int_{\mathrm{G_c}} 1/\sigma\,\nabla\times\boldsymbol{R}_{\mathbf{T},\mathrm{i}}\nabla\times\boldsymbol{R}'_{\mathbf{T}}\mathrm{dG_c}\int_t \mathrm{S}_{\mathbf{T},\mathrm{i}}S_{\boldsymbol{T},\mathrm{m}}\mathrm{dt} + \int_{\mathrm{G_c}}\mu\boldsymbol{R}_{\boldsymbol{T},\mathrm{i}}\boldsymbol{R}'_{\boldsymbol{T}}\mathrm{dG_c}\int_t {}^{dS_{T,\mathrm{i}}}\!/_{dt}\,S_{\boldsymbol{T},\mathrm{m}}\mathrm{dt}\right.\\
&\qquad\left.-\int_{\mathrm{G}}\mu\nabla\boldsymbol{R}_{\Omega,\mathrm{i}}\boldsymbol{R}'_{\boldsymbol{T}}\mathrm{dG}\int_t {}^{dS_{\Omega,\mathrm{i}}}\!/_{dt}\,S_{\mathbf{T},\mathrm{m}}\mathrm{dt}\right)\\
&=-\int_{\mathrm{G}}\mu\,\boldsymbol{T}_{0,\boldsymbol{x}}\mathrm{dG}\int_t {}^{dT_{0,t}}\!/_{dt}\,S_{\boldsymbol{T},m}\mathrm{dt}
\end{aligned} \tag{13}$$

$$\begin{aligned}
&\sum_{\mathrm{i}=1}^{\mathrm{m}}\left(\int_{\mathrm{G_c}} -\mu\nabla\boldsymbol{R}_{\Omega}{}'\boldsymbol{R}_{\mathbf{T},\mathrm{i}}\mathrm{dG_c}\int_t S_{\Omega,\mathrm{m}}S_{\mathbf{T},\mathrm{i}}\mathrm{dt} + \int_{\mathrm{G}}\mu\nabla\boldsymbol{R}_{\Omega,\mathrm{i}}\nabla\boldsymbol{R}_{\Omega}{}'dG\int_t S_{\Omega,\mathrm{i}}S_{\Omega,\mathrm{m}}\mathrm{dt}\right)\\
&=-\int_{\mathrm{G}}\mu\nabla\boldsymbol{R}_{\Omega}{}'\boldsymbol{T}_{0,\boldsymbol{x}}\mathrm{dG}\int_t S_{\Omega,m}T_{0,t}\mathrm{dt}
\end{aligned} \tag{14}$$

When identifying the time functions, the beforehand calculated space functions are set as being fixed, and the time functions are declared as unknowns, which results in a system of ordinary differential equations (ODE). The space test functions vanish and a combination of equations (11) and (12) with the $\boldsymbol{T}$-Ω-formulation results in equations (15) and (16).

$$\sum_{i=1}^{m}\left(\int_{G_c} 1/\sigma\,\nabla\times\boldsymbol{R}_{\mathbf{T},i}\nabla\times\boldsymbol{R}_{\mathbf{T},m}\mathrm{d}G_c \quad S_{\mathbf{T},i}+\int_{G_c}\mu\boldsymbol{R}_{\mathbf{T},i}\boldsymbol{R}_{\mathbf{T},m}\mathrm{d}G_c{}^{dS_{T,i}}/_{dt}\right.$$
$$\left.-\int_{G}\mu\nabla\boldsymbol{R}_{\Omega,i}\boldsymbol{R}_{\mathbf{T},m}\mathrm{d}G^{dS_{\Omega,i}}/_{dt}\right)$$
$$=-\int_{G}\mu\boldsymbol{T}_{0,x}\mathrm{d}G^{dT_{0,t}}/_{dt} \tag{15}$$

$$\sum_{i=1}^{m}\left(\int_{G_c}-\mu\nabla\boldsymbol{R}_{\Omega}{}'\boldsymbol{R}_{T,i}\mathrm{d}G_c \quad S_{\mathbf{T},i}+\quad\int_{G}\mu\nabla\boldsymbol{R}_{\Omega,i}\nabla\boldsymbol{R}'_{\Omega}\mathrm{d}G \quad S_{\Omega,i}\right)$$
$$=-\int_{G}\mu\nabla\boldsymbol{R}_{\Omega,m}\boldsymbol{T}_{0,x}dG \quad T_{0,t} \tag{16}$$

To solve the ODE, an implicit Euler method can be a suitable. The algorithm is shown in the following (PGD-Enrichment process)

```
PGD-Enrichment process
  R_T = { }, R_Ω = { } initialization of the space related reduced basis
  S_T = { }, S_Ω = { } initialization of the time related reduced basis
  While m <= maxMode and PGD-Enrichment is not converged
    Initialize S_T,m, S_Ω,m
    Repeat
        Solve space problem: R_T,m, R_Ω,m ← (13), (14)
        Solve time problem: S_T,m, S_Ω,m ← (15), (16)
        Normalize time functions: S_T,m ← S_T,m/‖S_T,m‖2, S_Ω,m ← S_Ω,m/‖S_Ω,m‖2
    Until ε_T (17) and ε_Ω (18) converged or maxNL is met
    Add R_T,m to R_T and R_Ω,m to R_Ω
    Add S_T,m to S_T and S_Ω,m to S_Ω
  End while
```

To improve the relative convergence of the enrichment process, one of the functions of each potential should be normalized to prevent cases in which one part of the decomposition tends to become infinitely small, while the other one diverges toward infinity. In this contribution, we arbitrarily choose the time functions to be normalized. This is particularly important for the $\boldsymbol{T}$-Ω-formulation owing to two unknown potentials. The alternative direction scheme is repeated until convergence or a maximum number of nonlinear iterations are met. The convergence of the single mode in the *kth* nonlinear iteration is computed by equations (17) and (18). The number of modes (NoM) is increased until the complete enrichment is converged or a maximum NoM (maxMode) are met. The convergence of the complete enrichment process is given by assessing the information content, which is enriched by the new mode compared to the previous enriched modes (Mueller *et al.*, 2019a, 2019b).

$$\epsilon_T = \frac{\|\boldsymbol{R}_{\mathrm{T}}{}^{\mathrm{k}}\boldsymbol{S}_{\mathrm{T}}{}^{\mathrm{k}} - \boldsymbol{R}_{\mathrm{T}}{}^{\mathrm{k-1}}\boldsymbol{S}_{\mathrm{T}}{}^{\mathrm{k-1}}\|_2}{\|\boldsymbol{R}_{\mathrm{T}}{}^{\mathrm{k-1}}\boldsymbol{S}_{\mathrm{T}}{}^{\mathrm{k-1}}\|_2} \tag{17}$$

$$\epsilon_{\Omega} = \frac{\|\boldsymbol{R}_{\Omega}{}^{\mathrm{k}}\boldsymbol{S}_{\Omega}{}^{\mathrm{k}} - \boldsymbol{R}_{\Omega}{}^{\mathrm{k-1}}\boldsymbol{S}_{\Omega}{}^{\mathrm{k-1}}\|_2}{\|\boldsymbol{R}_{\Omega}{}^{\mathrm{k-1}}\boldsymbol{S}_{\Omega}{}^{\mathrm{k-1}}\|_2} \tag{18}$$

3.3 Error evaluation

After the reduced representations have been achieved, the error compared to the reference simulation needs to be evaluated. Therefore, a physical error criterion, based on the Joule losses in the sample [equation (19)], is applied. Owing to the necessity of reference values, this is an *a posteriori* criterion.

$$\epsilon_J = \frac{P_{J,ref} - P_{J,MOR2}}{P_{J,ref\,2}} \tag{19}$$

4. Application

In this context, the $\boldsymbol{T}$-Ω-formulation is applied to solve an academic example of a conducting sample located inside a short coil (Figure 2). The model is computed with two different conductivities of 4 and 40 MS/m. Therefore, this example is similar to an induction furnace, in which the eddy currents can be used for heating a probe. The occurring eddy currents are proportional to the frequency and conductivity and will diffuse from the outside into the probe. To properly model the eddy currents, the skin depth has to be accurately discretized. The simulation frequency is arbitrarily set to 50 Hz and the sinusoidal current has an arbitrary magnitude of 100 A. The magnetic permeability is set to μ_0, and the reference solutions are obtained by a classic time-stepping simulation. The number of time steps (NoT) for the studied interval is set to 300.

4.1 Results – Proper Orthogonal Decomposition

In Figure 3, the evolution of the Joule losses are shown. For the sequential snapshot method (Figure 3a), six snapshots are sufficient to receive an error smaller than 2% for a given conductivity of 40 MS/m. It is obvious that the Joule losses are not accurate for lower

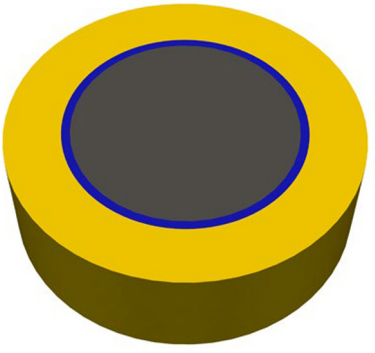

Figure 2.
Academic example of an eddy current problem (coil = yellow, sample = grey, airgap = blue)

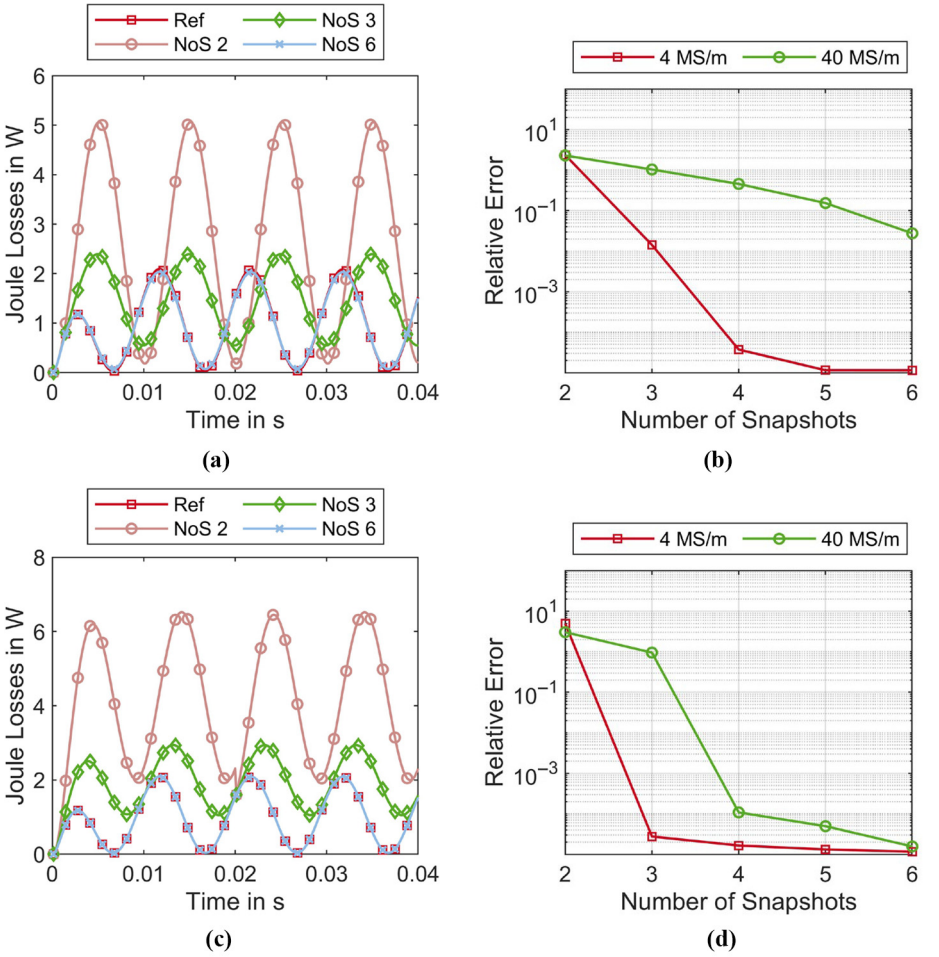

Figure 3.
Joule losses of the POD

Notes: (a) Joule losses versus time for POD taking sequential snapshot; (b) error of Joule losses for sequential POD; (c) Joule losses versus time for POD taking system-based snapshots; (d) error of Joule losses for system-based POD

numbers of snapshot. The Joule error [equation (19)] for the sequential snapshots is shown in Figure 3b. Owing to the transient eddy currents, which are proportional to the conductivity, less snapshots are necessary for an accurate representation of the losses for 4 MS/m compared to 40 MS/m. The convergence is given for both conductivities and is approximately linear.

The system-based approach produces a decomposition, which shows higher accuracy with less modes. The evolution of the system-based POD Joule losses behaves differently compared to the sequential approach. In Figure 3c, the corresponding losses for 40 MS/m are illustrated versus the time of two current periods. The convergence rate of the POD with system-based snapshots is much faster compared to the sequential snapshots. It can be

depicted from Figure 3d that three snapshots are enough to reproduce the eddy current losses for a conductivity of 4 MS/m with an error smaller than 3e-5, and for four snapshots the error drops below 2e-5. Also, the losses for the higher conductivity of 40MS/m are more accurate than those of the sequential snapshots approach. While the error of the sequential approach with four modes is higher than 20%, the error of the system-based approach is smaller than 1e-4. Comparing the Joule losses of the two different snapshot methods, it is noticeable that the system-based approach captures more relevant information of the transient effect with less NoS (Figure 1). This improvement in terms of accuracy comes with the price of more computations in the reference system. For the sequential approach, only NoS computations in the reference system have to be done, while the system-based approach needs the full first current period simulated in the reference system.

4.2 Results – Proper Generalized Decomposition

Owing to the direct decomposition of the PGD, the space and time modes can be analyzed directly. The first four computed space modes for a conductivity of 40 MS/m are shown in Figure 4. It can be depicted that the first mode is a uniformly rotating eddy current, while the second mode only has an eddy current on the side, which is decreasing toward the center of the sample.

The third mode shows an interesting phenomenon – the eddy currents at the top and bottom of the sample are rotating clockwise with a maximum at half of the sample radius. Moreover at the side of the sample, a counterclockwise rotating eddy current is visible. This can be interpreted as follows: the first mode acts like an eddy current in low conductive samples, while the second mode increases the eddy current in the edge region. The third

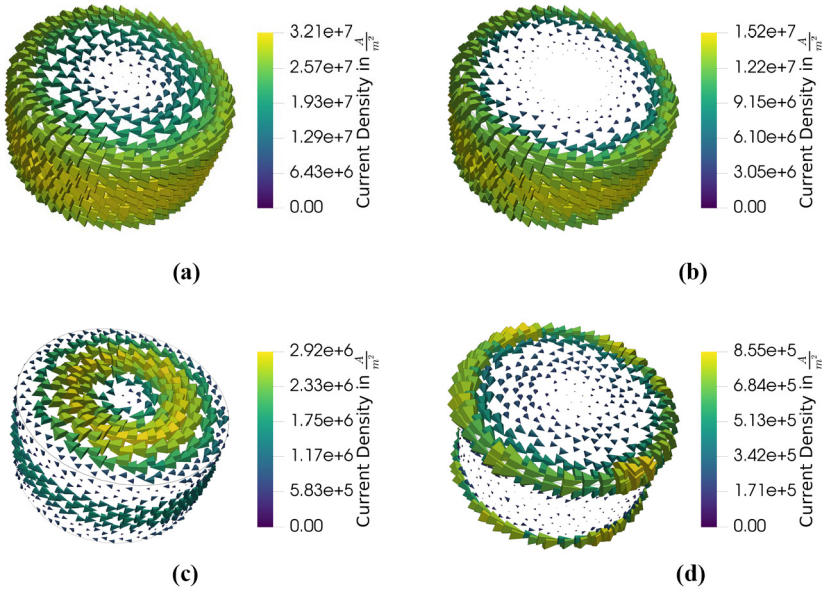

Notes: (a) First eddy current mode J_1; (b) second eddy current mode J_2; (c) third eddy current mode J_3; (d) fourth eddy current mode J_4

Figure 4.
Eddy current modes of the PGD

mode decreases the field in the middle of the sample. In combination with the enriched time functions, shown in Figure 5, the diffusion of the eddy current into the sample can be modeled by the linear combination given by equation (5). All functions show a transient behavior. In combination with the decreasing amplitude of the space modes, it can be assumed that the first two modes have a large impact on the overall behavior of the eddy currents, while the third and later diminish smaller errors of the transient simulation. The Joule losses of the PGD, depending on the NoM, are shown in Figure 6.

In contrast to the Joule losses computed with the POD, the first mode of the PGD contains the most dominant information of the electric vector potential T. The latter modes correct the amplitude and phase. The convergence of the error between the PGD and the reference losses is not as smooth as the convergence of the POD, but still a quasi-linear convergence rate can be depicted. For a conductivity of 4 MS/m, the first mode produces an error of approximately 20%, while the error of both POD methods with two snapshots is bigger than

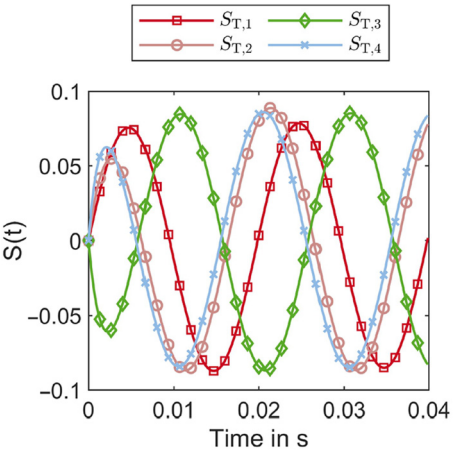

Figure 5.
Time functions of the PGD

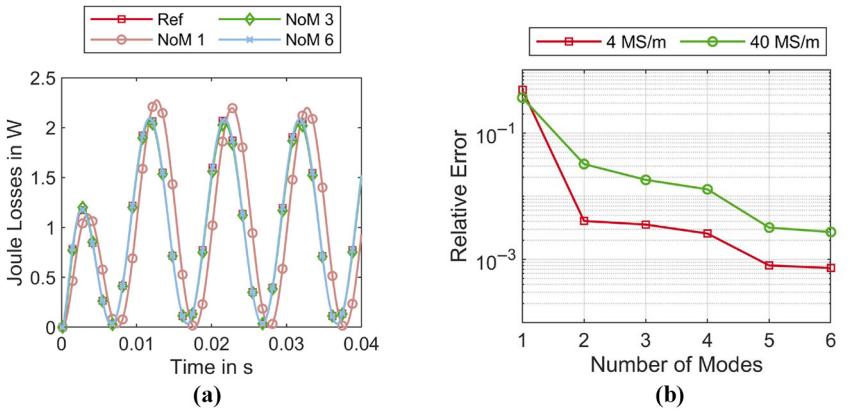

Figure 6.
Joule losses of the PGD

Notes: (a) Joule losses versus time for PGD; (b) error of Joule losses for PGD

100%. Similar to the POD methods, it can be seen that the error for the lower conductivities decreases faster than for the higher one.

4.3 Comparison of Proper Orthogonal Decomposition and Proper Generalized Decomposition

Consecutively, to the Joule loss evaluation, a direct comparison of the three MOR methods for a conductivity of 40 MS/m shall be done here. In Figure 7, the error [equation (19)] for all methods is illustrated, and two fundamental aspects can be recognized; first, the PGD produces accurate results with less modes than the sequential POD, and second, the overall accuracy of the POD is linearly improving, while the PGD does not converge as smoothly as the POD methods. The POD, regardless of the snapshot method, includes most relevant information of the solution space in the projection and thus is able to converge to the reference after enough modes are enriched. As the PGD does not use reference solutions, its convergence might be worse than the POD's because the basis of the PGD does not have to be orthogonal. However, the PGD has its advantages in terms of computational effort shown in Table 1. It only has to solve NoM·maxNL equation systems in the offline stage and consequently NoT·NoM multiplications in the online stage. For an even larger reduction, the decomposition can be improved leading to a better accuracy with less modes, as well as a better nonlinear convergence in the enrichment process by orthogonalization of the basis (Chinesta *et al.*, 2011), (Henneron and Clenet, 2016), (Mueller *et al.*, 2019a, 2019b). The POD nonetheless has fewer operations in the offline stage for sequential snapshot method and more operations in the online stage because the reference load vector has to be built and four

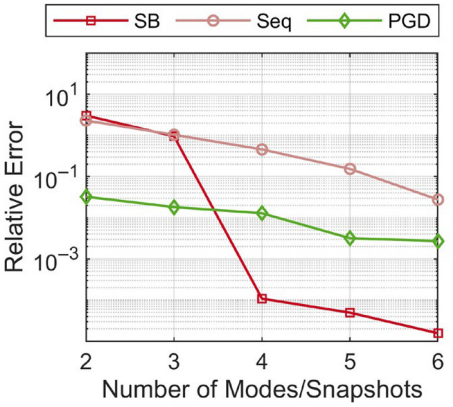

Figure 7. Error of the MOR techniques for $\sigma = 40$ MS/m

Operation	Ref	PGD	POD
Build ref. O(n^2)	NoT	NoM·maxNL	NoT
Solve ref. O(n^2)	NoT	NoM·maxNL	NoS
Solve red. O(NoS^2)	0	0	(NoT–NoS)
Multiplication O(n)	0	NoT·NoM	4·(NoT–NoS)

Table 1. Computational effort of a transient problem

projection operations are necessary. The first three projections are associated with equation (10), and the last is necessary to project the reduced solution back into the reference system. Furthermore, the PGD is able to cope with the "curse of dimensionality" by adding the material parameter of the conductivity to the decomposition (Chinesta *et al.*, 2011), (Chinesta *et al.*, 2014), (Krimm *et al.*, 2019).

5. Conclusions and further work

In this work, two MOR techniques have been used in context of an academic eddy current problem. By applying the POD and the PGD on the $\boldsymbol{T}$-Ω-formulation, an accurate reduced system could be achieved. The solutions for the eddy current losses and the distribution of the field quantities are equivalent to the reference solution. Further, a direct comparison between both methods is conducted. The influence of the selected snapshot and the influence of the conductivity on the convergence process are shown in detail, leading to the conclusion that both methods are well suited in this context. In future work, the conductivity will be directly added to the PGD and the movement, which is required for simulation of electrical machines and nondestructive eddy current testing.

References

Boehmer, S., Lange, E. and Hameyer, K. (2013), "Non-Conforming sliding interfaces for relative motion in 3D finite element analysis of electrical machines by magnetic scalar potential formulation without cuts", *IEEE Transactions on Magnetics*, Vol. 49 No. 5, pp. 1833-1836.

Chinesta, F., Keunings, R. and Leygue, A. (2014), *The Proper Generalized Decomposition for Advanced Numerical Simulations*, Springer International Publishing, Switzerland.

Chinesta, F., Ammar, A., Leygue, A. and Keunings, R. (2011), "An overview of the proper generalized decomposition with applications in computational rheology", *Mechanics*, *Journal of Non-Newtonian Fluid* , Vol. 166 No. 11, pp. 578-592.

Farzamfar, M., Rasilo, P., Martin, F. and Belahcen, A. (2015), "Proper orthogonal decomposition for order reduction of permanent magnet machine model", *in 18th International Conference on Electrical Machines and Systems (ICEMS), 25.- 28. Oct. 2015*, Pattaya City, Thailand.

Henneron, T. and Clenet, S. (2013), "Model order reduction of quasi-static problems based on POD and PGD approaches", *Eur. Phys. J. Appl. Phys*, Vol. 64 No. 2, pp. 1-7.

Henneron, T. and Clenet, S. (2014), "Model-Order reduction of Non-Linear magnetostatic problems based on POD and DEI methods", *IEEE Transactions on Magnetics*, Vol. 50 No. 2, pp. 33-36.

Henneron, T. and Clenet, S. (2016), "Application of the PGD and DEIM to solve a 3-D Non-Linear magnetostatic problem coupled with the circuit equations", *IEEE Transactions on Magnetics*, Vol. 52 No. 3, pp. 1-4.

Henneron, T., Mac, H. and Clenet, S. (2015), "Error estimation of a proper orthogonal decomposition reduced model of a permanent magnet synchronous machine", *IET Science, Measurement and Technology*, Vol. 9 No. 2, pp. 172-177.

Henneron, T., Le Menach, Y., Piriou, F., Moreau, O., Clenet, S., Ducreux, J. and Verite, J. (2007), "Source field computation in NDT applications", *IEEE Transactions on Magnetics*, Vol. 43 No. 4, pp. 1785-1788.

Krimm, A., Casper, T., Schops, S., De Gersem, H. and Chamoin, L. (2019), "Proper generalized decomposition of parameterized electrothermal problems discretized by the finite integration technique", *IEEE Transactions on Magnetics*, Vol. 55 No. 6, pp. 1-4.

Manges, J.B. and Cendes, Z.J. (1995), "A generalized Tree-Cotree gauge for magnetic field computation", *IEEE Trans. Magn*, Vol. 31 No. 3.

Montier, L., Pierquin, A., Henneron, T. and Clenet, S. (2017), "Structure preserving model reduction of Low-Frequency electromagnetic problem based on POD and DEIM", *IEEE Transactions on Magnetics*, Vol. 53 No. 6, pp. 1-4.

Mueller, F., Henneron, T., Clénet, S. and Hameyer, K. (2019a), "Error estimators for proper generalized decomposition in Time-Dependent electromagnetic field problems", *IEEE Transactions on Magnetics*, Vol. 56 No. 1, pp. 1-4.

Mueller, F., Crampen, L., Henneron, T., Clénet, S. and Hameyer, K. (2019b), "Model order reduction techniques applied to magnetodynamic scalar potential formulation", *19th International Symposium on Electromagnetic Fields in Mechatronics, Electrical and Electronic Engineering (ISEF) Book of Abstracts, 29.-31. Aug. 2019*, Lille, France.

Mukherjee, V., Far, M.F., Martin, F. and Belahcen, A. (2017), "Constrained algorithm for the selection of uneven snapshots in model order reduction of a bearingless motor", *IEEE Transactions on Magnetics*, Vol. 53 No. 6, pp. 1-4.

Nouy, A. (2010), "A priori model reduction through proper generalized decomposition for solving time-dependent partial differential equations", *Computer Methods in Applied Mechanics and Engineering*, Vol. 199 Nos 23/24, pp. 1603-1626.

Qin, Z., Talleb, H. and Ren, Z. (2016a), "A proper generalized decomposition-based solver for nonlinear magnetothermal problems", *IEEE Transactions on Magnetics*, Vol. 52 No. 2, pp. 1-9.

Qin, Z., Talleb, H., Yan, S., Xu, X. and Ren, Z. (2016b), "Application of PGD on parametric modeling of a piezoelectric energy harvester", *IEEE Transactions on Magnetics*, Vol. 52 No. 11, pp. 1-11.

Corresponding author
Fabian Müller can be contacted at: fabian.mueller@iem.rwth-aachen.de

For instructions on how to order reprints of this article, please visit our website:
www.emeraldgrouppublishing.com/licensing/reprints.htm
Or contact us for further details: **permissions@emeraldinsight.com**